Precision Optomechanics with a Particle in a Magneto-Gravitational Trap

Walter M. Klahold, Charles W. Lewandowski, Paul Nachman, Bradley R. Slezak, and Brian D'Urso

Montana State University, P.O. Box 173840, Bozeman MT, USA

ABSTRACT

Levitated particles are attractive systems for precision optomechanics due to their extreme isolation from their environment. Here we describe several experiments with microparticles in magneto-gravitational traps, which use a combination of diamagnetism and the earth's gravity. First, the center-of-mass motion of the particle can be cooled to temperatures far below the ambient temperature using feedback. Second, the change in the frequency of oscillation of the particle under the influence of field masses can be used to measure the Newtonian gravitational constant. Finally, the first steps towards producing and trapping silicon carbide microcrystals, which may contain optically-addressable defect centers, are reported.

Keywords: magnetic trapping, precision optomechanics, silicon carbide

1. INTRODUCTION

Levitated microparticles or nanoparticles in harmonic traps are elegant and attractive systems for ultra-sensitive force detection,[1,2] tests of fundamental physics,[3–5] and precision measurements. The leading approaches to levitation include optical traps,[6] Paul (oscillating electric field) traps,[7,8] and static magnetic field traps.[9–11] The three translational center-of-mass (COM) degrees of freedom of the trapped particle are typically probed, although some demonstrations have used rotational motion.[12–14] There has also been interest in trapping materials which host point defects, such as nitrogen-vacancy (NV) centers in diamond,[9,15] since the spin of the point defect can add an intrinsically quantum degree of freedom to the system. Interaction with such a quantum degree of freedom could enable the creation of motional quantum states of the COM of the particle, including macroscopically separated superposition (cat) states.[16]

In this paper, we present several projects using particles in magneto-gravitational traps.[9,10] These traps feature static fields and passive stability, even under ultra-high vacuum (UHV).[10] In Section 2, we outline our efforts to cool the COM motion of a trapped particle towards the quantum ground state; in Section 3 we describe progress towards a new measurement of the Newtonian gravitational constant using a large trapped microsphere and the time-of-swing method; and in Section 4, we report a new effort to produce and trap silicon carbide microcrystals to take advantage of optically-addressable defect centers in that material.

2. COOLING THE CENTER-OF-MASS MOTION

The motion of a particle in a magneto-gravitational trap can be described as that of a damped, driven harmonic oscillator. Left unaltered, the particle's motion will reach thermal equilibrium with its environment. It is typical to assign a temperature to the motion in a single translational degree-of-freedom from equipartition:

$$k_B T_i = m\omega_i^2 \langle x_i^2 \rangle \tag{1}$$

where k_B is the Boltzmann constant, T_i is the temperature, m is the particle's mass, ω_i is the natural angular frequency, and x_i is the displacement, with subscripts denoting the degree-of-freedom (x, y, and z for transverse, vertical, and axial, respectively). At ambient temperature, due to the small masses of particles used ($m \approx 1\,\mathrm{pg}$)

Further author information: (Send correspondence to B.D.)
B.D.: E-mail: durso@montana.edu, Telephone: 1 406 994 3456

and low frequencies ($\omega_i/2\pi < 100\,\mathrm{Hz}$), the amplitude of a particle's motion is quite large compared to its diameter. To better control the motion, cold damping[17] is applied to the particle's motion: energy is removed, decreasing the amplitude and thus the temperature of that motion. In this way, we define cooling the COM motion as the removal of energy from its translation. Ideally, this process can cool the motion to its quantum-mechanical ground state.[18]

Our magneto-gravitational traps consist of a pair of SmCo permanent magnets sandwiched between ferromagnetic pole pieces and arranged in a quadrupole configuration, fully contained within a vacuum chamber.[9,10] For COM cooling experiments, we use a version of the trap with a physical trapping region of approximately $50\,\mu\mathrm{m} \times 150\,\mu\mathrm{m} \times 250\,\mu\mathrm{m}$, corresponding to the size of the gaps between the pole pieces in the transverse (x) and vertical (y) directions and the length of the top pole piece along the axial (z) direction, respectively. These dimensions, combined with the strong magnetic field present and the diamagnetic susceptibility of the silica microspheres, generate oscillation frequencies of approximately $\omega_x/2\pi \approx 60\,\mathrm{Hz}$, $\omega_y/2\pi \approx 100\,\mathrm{Hz}$, and $\omega_z/2\pi \approx 10\,\mathrm{Hz}$. A depiction of the trap and the defined axes is shown in Fig. 1.

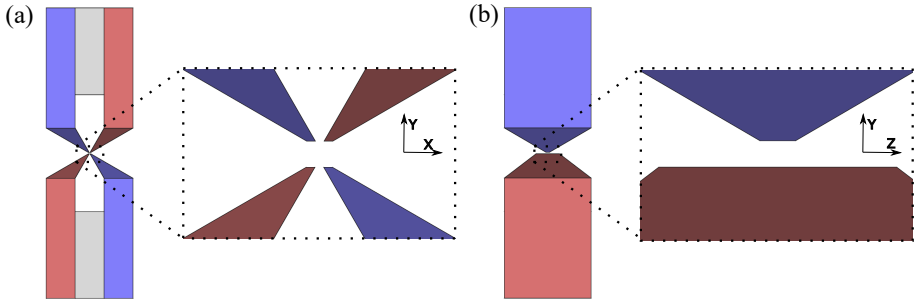

Figure 1. The trap used for COM cooling experiments is depicted. Blue and red shaded pole pieces correspond to south and north poles, respectively. (a) The trap viewed from the side, showing the quadrupole arrangement of the magnets (gray) and pole pieces and defining the transverse (x) and vertical (y) directions. (b) The trap viewed from the front, defining the vertical (y) and axial (z) directions.

We load (via a multi-step process at atmospheric pressure) a single silica microsphere, typically of diameter $d = 1.54\,\mu\mathrm{m}$, in this trap. The residual gas in the chamber is then reduced to decrease the frequency of collisions with air molecules. Due to the passive stability of the trap, the pressure in the trapping environment is reduced to the UHV range without any monitoring or control of the sphere's motion, with pressures of $P \approx 1 \times 10^{-10}\,\mathrm{Torr}$ regularly achieved. The charge of a sphere can be controlled at the single-electron-charge level, and the net charge on the sphere can be reduced to zero to minimize electrical interference and fluctuation-dissipation mechanisms involving induced currents in the pole pieces.

Light from two diode lasers (at different wavelengths) is loosely focused onto the microsphere. The scattered light from the illumination beam (at 830 nm) is used to image the sphere onto a quadrant photodiode detector, while amplitude-modulated light from the control laser (at 660 nm) manipulates the particle's motion via radiation pressure. Difference currents from the photodiode quadrants generate electrical signals proportional to the sphere's displacements in the y-z plane. Analog filters (narrowband active differentiators) use these displacement signals to generate signals proportional to the sphere's velocity. These velocity signals are used to amplitude-modulate the control laser, providing negative feedback to damp the sphere's motion.

To report the degree of cooling achieved, we assign an effective temperature T_i to the motion using Eq. 1. To date, we have demonstrated effective temperatures in the vertical and axial directions of $T_y = 1.2\,\mathrm{mK}$ and $T_z = 0.6\,\mathrm{mK}$ (with preliminary new results of $T_y = 1.0\,\mathrm{mK}$ and $T_z = 0.14\,\mathrm{mK}$), a factor of $\sim 10^6$ below ambient temperature ($T \approx 300\,\mathrm{K}$).[10] These temperatures approach the largest amount of cooling of COM motion in documented optical trapping experiments.[19–21] While the average energies of these motions are still significantly larger than their quantum-mechanical ground state energies, these results confirm a system with excellent environmental isolation and high degree of control, allowing continued development in COM cooling as well as other endeavors.

3. MEASURING THE NEWTONIAN GRAVITATIONAL CONSTANT G

Since the first laboratory measurement of the Newtonian gravitation constant G by Henry Cavendish more than 200 years ago,[22] over 200 other measurements have been made using a variety of techniques,[23,24] many of which are based on the torsion balance used by Cavendish.[25] Measurements have also been done by beam balances,[26] double pendula,[27] and atom interferometry.[28] Despite this long history of measurements, the precision to which G is known is still poor compared to other fundamental constants,[25] a consequence of the weakness of gravity relative to the other fundamental forces. Measuring G to a precision on the order of 10 ppm is very difficult and measurements often disagree by several standard deviations.[27,29,30]

Our unique magneto-gravitational trap can provide a method of performing a time-of-swing measurement[30] of the Newtonian gravitational constant G in ultra-high vacuum which avoids many of the systematic errors associated with previous experiments (e.g. inelasticity in the fiber used to suspend the test mass in a torsion balance[31]). The trapped diamagnetic microsphere with mass m oscillates with angular frequencies ω_x, ω_y, ω_z in the x, y, and z directions, respectively. When two field masses M are placed a distance d from the equilibrium position of the test mass (similar to Fig. 2), the spring constant of the oscillating mass changes, thus changing

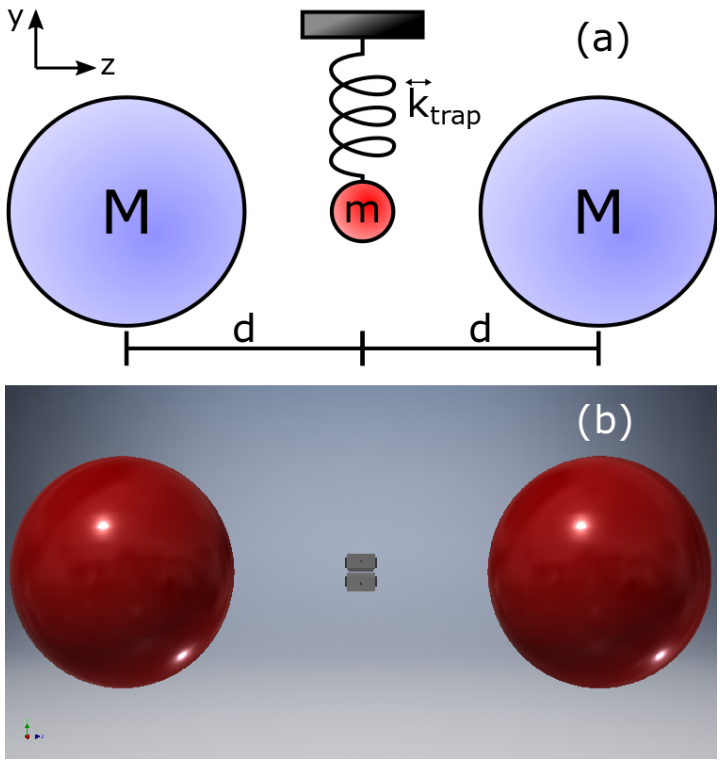

Figure 2. (a) A simplified illustration of the time-of-swing method. The test mass m is suspended between two field masses M by a harmonic (magneto-gravitational) trap with spring constants k_x, k_y, and k_z. The difference in oscillation frequency in the z direction gives a measurement of G via the change in the spring constant. (b) A rendering of the magneto-gravitational trap with two field masses.

the frequency of motion.

For small displacements from equilibrium Δx, Δy, and Δz, the spring constant after the addition of the field masses along the z direction is

$$k_z' = -\frac{dF_z}{dz} = k_z - \frac{4GMm}{d^3}\left[1 - 3\left(\frac{\Delta x}{d}\right)^2 - 3\left(\frac{\Delta y}{d}\right)^2 + 6\left(\frac{\Delta z}{d}\right)^2 + \cdots\right], \tag{2}$$

where k_z is the spring constant of the magneto-gravitational trap alone in the z direction. Dropping anharmonic terms, Eq. 2 simplifies to

$$k'_z = k_z - \frac{4GMm}{d^3}. \tag{3}$$

The gravitational effect of the two field masses changes the frequency of the test mass from $\omega_z = \sqrt{k_z/m}$ to $\omega'_z = \sqrt{k'_z/m}$. The final frequency of the test mass is

$$\omega'_z = \sqrt{\frac{k_z}{m} - \frac{4GM}{d^3}} = \sqrt{\omega_z^2 - \frac{4GM}{d^3}} \approx \omega_z - \frac{2GM}{\omega_z d^3} \qquad \text{or} \qquad G = \frac{d^3}{4M}\left(\omega_z^2 - (\omega'_z)^2\right) \tag{4}$$

Thus, to measure G, we simply need to know the frequency of the test mass before and after the addition of the field masses, M, and the distance from the field masses to the equilibrium position of the test mass.

3.1 Loading and Trapping of Large Particles

In order to reduce thermal motion of the microsphere, larger microspheres are preferable to use in the time-of-swing measurement. In the past, we have successfully loaded and trapped microspheres up to approximately 8 µm in diameter in our traps. We have not been able to trap larger microspheres in the traps used for cooling (see Section 2) reliably. A new loading method has been developed to allow trapping of larger microspheres.

A piece of insulating polyimide tape was placed on the tip of an ultrasonic horn and charged by rubbing against polyester fabric. Large microspheres (25 µm to 63 µm diameter) are then able to be electrostatically held on the tip. An oscillating (AC) voltage is placed on the pole pieces of the trap in a quadrupole configuration to make a linear Paul trap[32,33] for the microspheres, which carry residual charge from the loading process. The AC quadrupole trap is much stronger than the magneto-gravitational trap, allowing large microspheres to be levitated in the center of a trap with larger gaps between the pole pieces. Trapping parameters for the Paul trap were determined experimentally for a range of microsphere sizes. A constant (DC) voltage is applied between the top and bottom of the trap to help center more massive microspheres. Typical values for trapping parameters for 63 µm microspheres (Cospheric BSGMS-2.2) are approximately 500 VAC amplitude at 300 Hz, and a range of 20-35 VDC. These are the largest microspheres we have been able to trap.

To achieve ultra-high vacuum with no feedback cooling of the microsphere, the Paul trap needs to be shut off before pumping on the chamber. To keep the large microspheres in the center of the trap, the DC voltage is adjusted so the microsphere remains trapped by the combination of the DC field and magneto-gravitational trap as the Paul trap voltage is slowly turned off.

Because of the method used to load these microspheres, excess microspheres that are not trapped contaminate the chamber and stick to the pole pieces of the trap. Since all of the microspheres are charged, these contaminants distort the local trapping potential seen by the charged microspheres successfully trapped and make the motion anharmonic. Defects in the pole pieces have a similar effect on the microspheres. The dimensions of the trap were increased to help minimize this issue. The dimension in the x direction was increased to approximately 250 µm and that in the y direction to approximately 650 µm (Fig. 3). The trapped microspheres are now farther away from the contaminants and defects and are thus less affected by them.

To ensure that the Brownian motion of the microsphere is insignificant, the amplitude of the motion should be much greater than the Brownian motion. Furthermore, a large oscillation amplitude will tend to smooth out local potential changes due to contaminants and defects on the pole pieces. To support a large oscillation amplitude, the dimension of the trap in the z direction is approximately 26 mm, much larger that that of the traps used in Section 2.

3.2 Frequencies of the Trapped Particles

As evident in Eq. 4, the change in frequency due to the field masses increases in magnitude by increasing M, decreasing d, or lowering the oscillation frequency of the microsphere. M cannot be made arbitrarily large to the finite density of available materials, the challenge of precisely machining large parts, and difficulty of handling extremely heavy masses. The distance d is further limited because the field masses have to remain outside of the trapping region, and, more practically, outside the vacuum chamber that houses the trap and test mass, as we

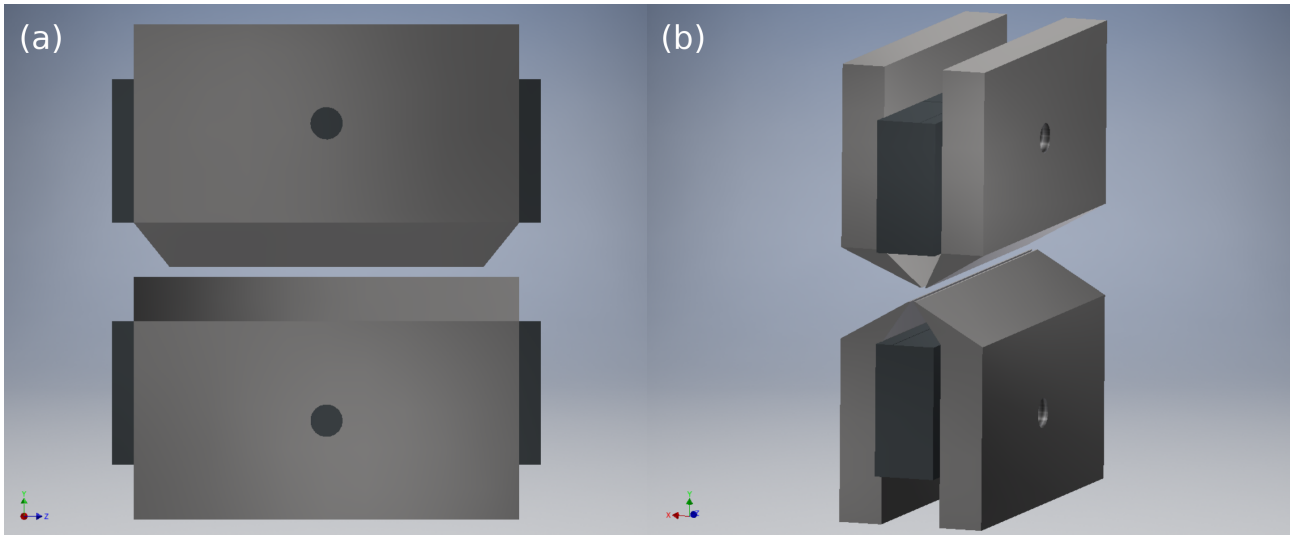

Figure 3. (a) The view of the trap in the y-z plane. The length of the trap in the z direction is approximately 26 mm to allow for large amplitude oscillations. (b) The trapping region is defined by four pole pieces that concentrate the magnetic field to a small region of approximately 250 µm in the x direction and 650 µm in the y direction.

will need to place and remove the field masses without venting the chamber to obtain measurements with and without the masses. The one parameter that could be broadly tuned is the oscillation frequency.

Our typical trap design[10] results in an anharmonic potential near the edges of the trap and in particular an increase in the oscillation frequency at large amplitudes of oscillation in the z direction. By making the trap longer in the z direction and making the vertical gap larger, the potential in the center of the trap is flattened, lowering the frequencies of oscillation and enabling a much larger harmonic oscillation amplitude in the z direction. In our cooling experiments (see Section 2), the oscillation frequency in the z direction is approximately 10 Hz and in the y direction approximately 50 Hz. In the trap developed for measuring G, we have measured $\omega_y/2\pi \approx 9$ Hz and $\omega_z/2\pi \approx 0.6$ Hz for a small amplitude of oscillation of approximately 100 µm. The microsphere with this frequency is pictured in Fig. 4. With further improvements, we hope to achieve a frequency in the z direction of 0.1 Hz or less.

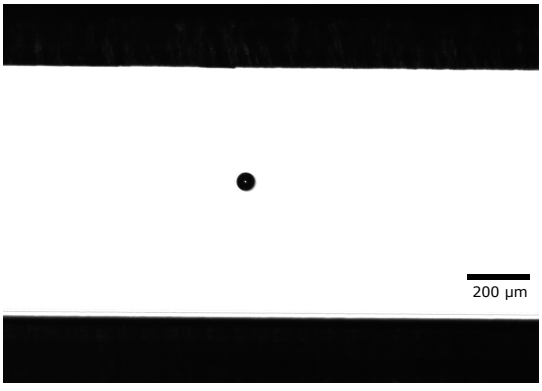

Figure 4. A 59 µm diameter microsphere levitated in the large magneto-gravitational trap. The measured frequencies for this particle are $\omega_z/2\pi \approx 0.6$ Hz and $\omega_y/2\pi \approx 9$ Hz.

4. TRAPPING SILICON CARBIDE MICROCRYSTALS

In order to introduce SiC particles into our levitation experiments, we have developed several key steps to process bulk SiC into particles with sizes and shapes well-suited to our optical feedback and control schemes. The first step in this process is the crushing and grinding of bulk material into micrometer-size particles. To do this we use a tool steel mortar and pestle to manually grind up a small wafer of material. The process is slow, and the resulting particle sizes are widely distributed (most are between one and a few hundred micrometers), although very little material is lost in the process. A few square centimeters of a $\sim 600\,\mu$m thick, ultra-pure (nitrogen concentration of $3 \times 10^{13}\,\mathrm{cm}^{-3}$) homoepitaxial 4H SiC wafer were used as the starting material, and we have found that this yielded enough powder to last many attempts at loading our magneto-gravitational traps.

Another issue with this method is the resulting contamination of the powder with ferric particulates from the tool-steel-based mortar and pestle. SiC particles with these contaminants embedded in them are attracted to the pole pieces instead of the intended trapping region, but even if the contaminants did not adhere to the SiC, they would likely accumulate on the magnets and pole pieces after many loading attempts. We have found that a simple wet etching routine is sufficient to remove tool steel particles from the SiC powder. The procedure we followed was to immerse the contaminated powder in concentrated hydrochloric acid (to which SiC is inert[34]), agitating the suspension several times over the course of a few hours before allowing the etching to proceed undisturbed for a few days. After this, the hydrochloric acid was decanted and the powder rinsed with deionized water and allowed to dry in air. Finally, the powder was again placed into concentrated hydrochloric acid for several hours, rinsed in deionized water, and air-dried. In Fig. 5 is shown a $\sim 50\,\mu$m particle of SiC that has

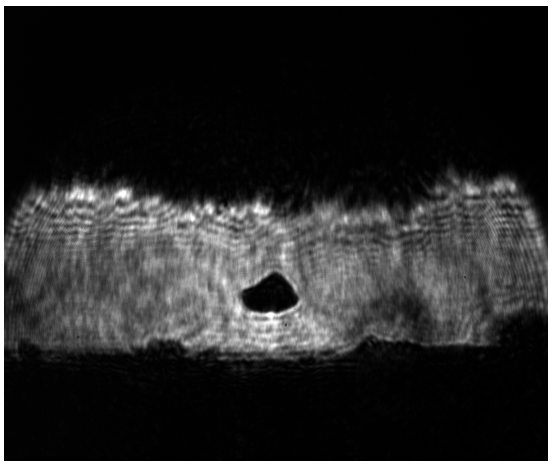

Figure 5. Image of a $50\,\mu$m particle of 4H SiC suspended in a magneto-gravitational trap. The image is taken along the transverse direction of the trap. The two dark regions at the top and bottom of the image are the top and bottom pairs of pole pieces, and the $\sim 120\,\mu$m gap between is occupied by the particle, which is back-illuminated with a laser. This particle came from a batch of 4H SiC powder produced according to the method described in the text.

been successfully loaded into one of our magneto-gravitational traps following the above wet etching procedure, whereas, before this procedure, particles from the same batch of powder were seen to be attracted to the pole pieces upon entering the trapping region.

4.1 Particle Etching and Reshaping

The particles produced from the grinding method described above are often irregular in shape and exhibit faceted surfaces that are indicative of conchoidal fractures. The facets themselves are typically marred by large scratches or cleavage steps, but even for relatively flat faces the surface appears somewhat opaque, indicating near-micron scale surface roughness. The surface roughness and irregularity can be problematic for our trapping experiments for several reasons. It can: reduce the coupling efficiency of light into or out of the particle, which is necessary for optically addressing embedded defects; introduce surface defects which might luminesce or otherwise interfere with the embedded defects of interest; give rise to an orientation-dependent angular-scattering distribution,

which could interfere with position detection; and enable the incident light field to drive particle rotations, which in turn could excite the particle's COM motion should any coupling exist between the particle's rotational and translational degrees of freedom.[12–14] In terms of the lowest COM motion effective temperature we can achieve with our current trap design, we have observed at least three orders of magnitude improvement when trapping silica microspheres[9] instead of nanodiamonds,[10] which can be attributed at least in part to the nanodiamonds being irregularly shaped.

Were it possible to reshape the SiC particles through an additional etching step, we expect a similar improvement might be made. Despite silicon carbide's chemical inertness, etching of SiC is a problem that has been extensively explored. We have experimented with two techniques to etch our SiC particles: dry hydrogen etching and wet oxidative etching. To our knowledge, these methods have only been applied to bulk material rather than powder, and our preliminary findings for powder show a marked increase in etch rates over those observed for bulk SiC. At this stage, both techniques are adequate for particle size reduction, but it is the wet oxidative etching method which shows greater promise for producing smoother surfaces and more regular shapes in the particles.

4.1.1 Hydrogen Etching

Hydrogen etching of SiC has been investigated as far back as the 1960's[35–37] and is in common use today as a means to remove polishing damage from substrates and produce atomically flat surfaces[38,39] for chemical vapor deposition.[40,41] We have modeled our hydrogen etching experiments after those of Ishida and Yoshida,[42] in which etching was performed on 8° off-axis 4H SiC substrates inside a vertically blown CVD reactor where argon was used as a carrier gas for the hydrogen. Under their experimental conditions, it was determined that the etching proceeds with silicon sublimation followed by hydrocarbon formation and desorption.

We have attempted to reproduce these conditions using an aluminum oxide tube furnace with a 1500°C maximum temperature. In the experiments performed by Ishida and Yoshida,[42,43] etching was carried out in vacuum in order to promote the sublimation of silicon, and so we connected our furnace tube via vacuum-compatible fittings to a pair of gas cylinders at the inlet and a vacuum pump at the outlet. While the furnace was maintained at the desired etching temperature, a 95% argon / 5% hydrogen mix was supplied from one of the cylinders at a fixed flow rate and pressure, whereas ultra-high purity argon from the second cylinder was supplied during the period of heating up and cooling down to prevent oxide formation. In the early stages of our experiments, SiC powder samples were supported inside the furnace tube with either SiC or graphite furniture, but after observing minimal etching of the powder it was determined that the furniture was competing with the powder for hydrogen. This observation is compatible with that by Ishida and Yoshida in which etching is limited by hydrogen mass transport when its concentration in the argon carrier gas is in the vicinity of 5%.[42] Afterwards, all of our etching experiments were carried out with samples held in aluminum oxide boats, at which point we observed a marked increase in etch rate.

The results from one of these later etching experiments is given in Fig. 6, which shows a microscope image of a rather large ($\sim 600\,\mu m$) particle fractured off of a $359\,\mu m$ thick wafer of boule, 4H SiC both before and after hydrogen etching and at different magnifications. This particle was not produced by the grinding method described earlier, but was snapped off of a wafer as a large chunk so that images of the same particle both before and after etching could be directly compared. However, the facets resulting from the conchoidal fractures are similar in structure to those of the particles produced from grinding. In this case etching was carried out at 1500 °C and 20 Torr for 45 min and with the argon-hydrogen mixed gas flowing at 730 sccm. From the low magnification images, it can be estimated that an etch rate of nearly $100\,\mu m\,h^{-1}$ was achieved. This is to be compared with the $\sim 2\,\mu m\,h^{-1}$ etch rate obtained by Ishida and Yoshida for a similar combination of temperature, pressure, and H_2 concentration, but with a substantially higher flow rate (15,000 sccm). This would seem to contradict the linear dependence of etch rate on flow rate predicted by Ishida's and Yoshida's analysis of the hydrogen etching kinetics,[42,43] although one should note that geometrical differences between our furnace and their CVD reactor prevent a direct comparison of the observations. It is also possible that, after we removed all SiC and carbon furniture from our furnace, their reactor contains more materials that would compete with SiC for hydrogen. Differences in the samples of SiC themselves might serve as another explanation. In particular, the many facets and grooves seen in the pre-etch images of Fig. 6 may very well serve to seed enhanced etching in a way that would not be observed for the planar geometry substrates studied by Ishida and Yoshida.

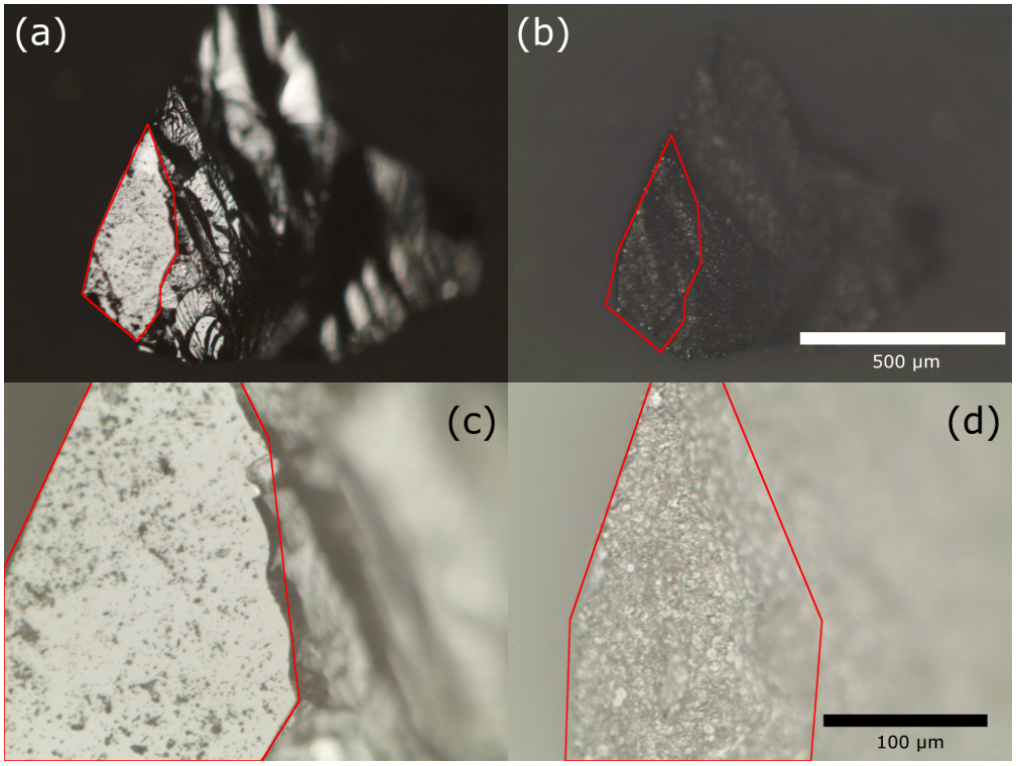

Figure 6. 600 µm 4H SiC particle viewed under an optical microscope (a and c) before and (b and d) after hydrogen etching at 1500°C for 45 min. The white scale bar corresponds to the top two images and the black scale bar corresponds to the bottom two images. Hydrogen was introduced into the furnace as a 5% mixture with an argon carrier gas and flowed at a rate of 730 sccm. A mechanical pump at the outlet of the furnace tube was used to reduce the pressure to 20 Torr and enhance the rate of silicon sublimation. An etch rate of about 100 µm h^{-1} is estimated from the overall size reduction of the particle. The highlighted regions indicate either a (0001) or $(000\bar{1})$ face.

Aside from the substantial reduction in size, the particle in Fig. 6 also exhibits a substantial increase in surface roughness. Interestingly, this roughness appears to be uniform over the entirety of the particle's surface, irrespective of the crystallographic orientations of the etched facets. For instance, the facet highlighted in red in the figure is known to be either a (0001) or $(000\bar{1})$ face, and yet it seems to exhibit the same roughness as the other facets resulting from conchoidal fractures. This is surprising given the fact that even the parallel (0001) and $(000\bar{1})$ planes would present a different bonding environment to the adsorbed hydrogen and have been observed in other studies to exhibit different etch rates and post-etching morphologies.[35,36] Similar surface roughness can also be seen in etched SiC particles produced from grinding. In Fig. 7 are shown representative images of these particles before and after hydrogen etching at 1450 °C for 1 h. Whereas the particles before etching exhibit rather smooth facets, the surfaces of the particles after etching show a surface roughness of a few micrometers in size. Additionally, the overall shapes of the particles remain quite irregular. At this stage we have observed no signs that effective smoothing and reshaping of the particles can occur with hydrogen etching, although more experimentation is needed to reach any definitive conclusion.

4.1.2 Wet Oxidation

Following our preliminary results with hydrogen etching, it was decided that a more viable strategy might be to pursue a wet oxidative etching technique in which removal of material from the surface is accomplished through its conversion to silica, which is subsequently volatilized. This can be accomplished by heating the SiC to high temperatures in an environment containing water vapor, which serves to both oxidize the SiC and volatilize the resulting silica:[44–46]

$$\mathrm{SiC} + 3\mathrm{H_2O(g)} = \mathrm{SiO_2} + 3\mathrm{H_2(g)} + \mathrm{CO(g)} \tag{5}$$

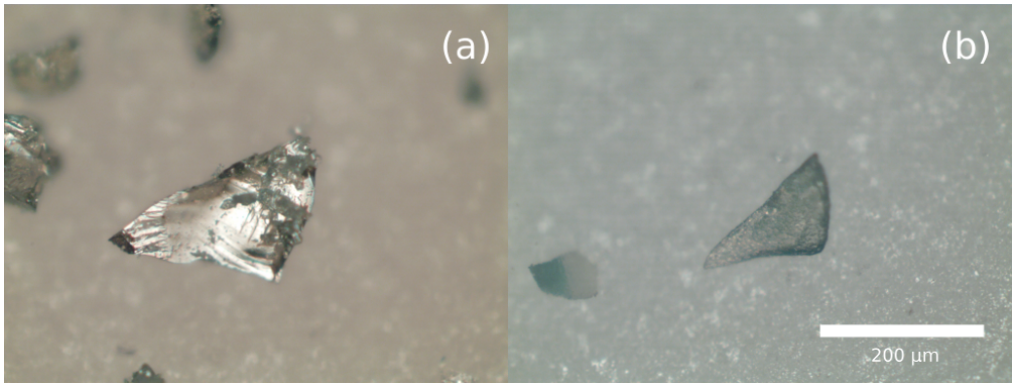

Figure 7. Representative images of particles produced from the mechanical grinding technique described in the text (a) before (b) and after hydrogen etching for 1 hour at 1450 °C (note that the triangular particle shown in (a) may not be the same as the triangular particle shown in (b)). The gas flow and pressure are the same as for Fig. 6.

$$SiO_2 + 2H_2O(g) = Si(OH)_4(g) \tag{6}$$

The choice to pursue this technique was made based on the expectation that the etching rate might be limited under certain conditions by the diffusion of water vapor through an amorphous oxide layer, which in turn could lead to an overall rounding of edges and points. In fact, it has been found that wet oxidative etching of SiC by water vapor follows a paralinear rate equation:[45,46]

$$\frac{dx}{dt} = \frac{k_p}{2x} - k_l, \tag{7}$$

where the first term on the right represents a parabolic rate law for oxide formation, which can be derived on the assumption that diffusion through the oxide layer is the rate-limiting step.[47,48] Volatilization of the oxide layer is accounted for by the second term on the right. Here, x is the oxide thickness, k_p is a rate constant related to the diffusion of the oxidant through the oxide layer, k_l is the rate of oxide volatilization, and t is the duration of oxide formation and volatilization. A steady-state solution to Eq. 7 for which the oxide is volatilized at the same rate as it is formed results in a limiting oxide thickness

$$x_L = \frac{k_p}{2k_l} \tag{8}$$

and a linear rate of net material recession which is proportional to the volatilization rate k_l.[45,46]

The rate constants k_p and k_l have been measured in several different furnaces by Opila and Hann for a range of temperatures, flow rates, and water vapor partial pressures.[45,46] We have used their experiments as a starting point to our investigations, although we expected there to be differences in the observed recession rates as was the case for the hydrogen etching. Oxidation of our SiC powder was again performed in our tube furnace, which was reconfigured to mix water vapor in with the flow gas. This was accomplished by bubbling argon through a heated flask of deionized water, the outlet of which was connected to one end of the furnace tube. Gas flowing from of the outlet of the furnace tube was bubbled through a room temperature flask of deionized water, which acted as a one way valve and flow indicator. In this case, no vacuum pump was attached to the outlet, as all our experiments with this oxidation technique were carried out at atmospheric pressure.

The oxidation procedure proceeds as follows: while the furnace would warm up to its set point temperature, a 120 sccm flow of ultra-high purity argon is bubbled through the inlet flask of deionized water, which is kept at room temperature. As soon as the furnace reached its set point temperature, the flow of argon is increased to 200 sccm and the inlet flask is heated to ~ 80 °C, corresponding to a 355 Torr partial pressure of water vapor.[49] The temperature is maintained for a few hours, during which time we assume most of the oxidation occurs. Afterwards, both the furnace and the inlet flask is allowed to cool to room temperature over a period of several

hours while argon continues to flow through the system at a rate of 120 sccm. As with hydrogen etching, batches of 4H SiC powder are oxidized in aluminum oxide boats.

Comparisons of the particles before and after oxidation are shown in Fig. 8 for four separate oxidation temperatures from 1200 to 1500 °C, with the dwell time fixed at 2 h. After oxidation at 1200 °C, thin film interference at the surface of the particles suggests a thin ($\sim$ 100 nm) oxide has formed, although the overall shape and morphology of the particle appears to be preserved. This appears to be the case for particles oxidized at 1300 °C as well, although higher order interference fringes indicate a thicker oxide. At 1400 °C we observe the first signs of surface smoothing and rounding of edges, although the net removal of material at this stage is estimated to be only a few microns. Particles oxidized at 1500 °C show the clearest evidence of surface smoothing and reshaping. Virtually none of these particles exhibit the sharp edges and well-defined grooves characteristic of the unetched particles. A few of the particles from this oxidation run have retained their original, irregular shapes, but the majority seem to have tended towards a more spheroidal shape as material has been removed. In general these particles appear to be more translucent, indicating that the original, micron-scale surface roughness has been successfully smoothed. The overall size reduction of the particles is estimated to be no more than a few tens of micrometers. To determine the thickness of the resulting silica overlayer, we placed one of the larger particles into a hot bath of aqueous KOH for several hours to etch away the silica and leave behind the SiC core. A visual comparison of the particle under our optical microscope before and after KOH etching indicated no observable change in size, and so the silica overlayer on this batch of particles was likely to be at most a few micrometers thick. With further experimentation, it may be possible to precisely control the oxide thickness for the purpose of, e.g., forming an anti-reflective coating on the particles. In any case, our primary goal of reshaping the particles and reducing surface roughness appears to have been nearly met with these preliminary results for oxidative etching at 1500 °C.

ACKNOWLEDGMENTS

We would like to thank W. J. Choyke and R. P. Devaty for helpful discussions and for providing SiC samples. This material is based upon work supported by the National Science Foundation under Grant No. 1757005, 1827071, and 1707789, and a block gift from the II-VI Foundation.

REFERENCES

[1] Ranjit, G., Cunningham, M., Casey, K., and Geraci, A. A., "Zeptonewton force sensing with nanospheres in an optical lattice," *Phys. Rev. A* **93**(5), 053801 (2016).

[2] Monteiro, F., Ghosh, S., Fine, A. G., and Moore, D. C., "Optical levitation of 10-ng spheres with nano-g acceleration sensitivity," *Phys. Rev. A* **96**(6), 063841 (2017).

[3] Moore, D. C., Rider, A. D., and Gratta, G., "Search for millicharged particles using optically levitated microspheres," *Phys. Rev. Lett.* **113**(25), 251801 (2014).

[4] Goldwater, D., Paternostro, M., and Barker, P., "Testing wave-function-collapse models using parametric heating of a trapped nanosphere," *Phys. Rev. A* **94**(1), 010104 (2016).

[5] Moore, D. C., "Tests of fundamental physics with optically levitated microspheres in high vacuum," in [*Optical Trapping and Optical Micromanipulation XV*], **10723**, 107230H, International Society for Optics and Photonics (2018).

[6] Ashkin, A., "Acceleration and trapping of particles by radiation pressure," *Phys. Rev. Lett.* **24**(4), 156 (1970).

[7] Millen, J., Fonseca, P., Mavrogordatos, T., Monteiro, T., and Barker, P., "Cavity cooling a single charged levitated nanosphere," *Phys. Rev. Lett.* **114**(12), 123602 (2015).

[8] Fonseca, P., Aranas, E., Millen, J., Monteiro, T., and Barker, P., "Nonlinear dynamics and strong cavity cooling of levitated nanoparticles," *Phys. Rev. Lett.* **117**(17), 173602 (2016).

[9] Hsu, J.-F., Ji, P., Lewandowski, C. W., and D'Urso, B., "Cooling the motion of diamond nanocrystals in a magneto-gravitational trap in high vacuum," *Sci. Rep.* **6**, 30125 (2016).

[10] Slezak, B. R., Lewandowski, C. W., Hsu, J.-F., and D'Urso, B., "Cooling the motion of a silica microsphere in a magneto-gravitational trap in ultra-high vacuum," *New. J. Phys.* **20**, 063028 (2018).

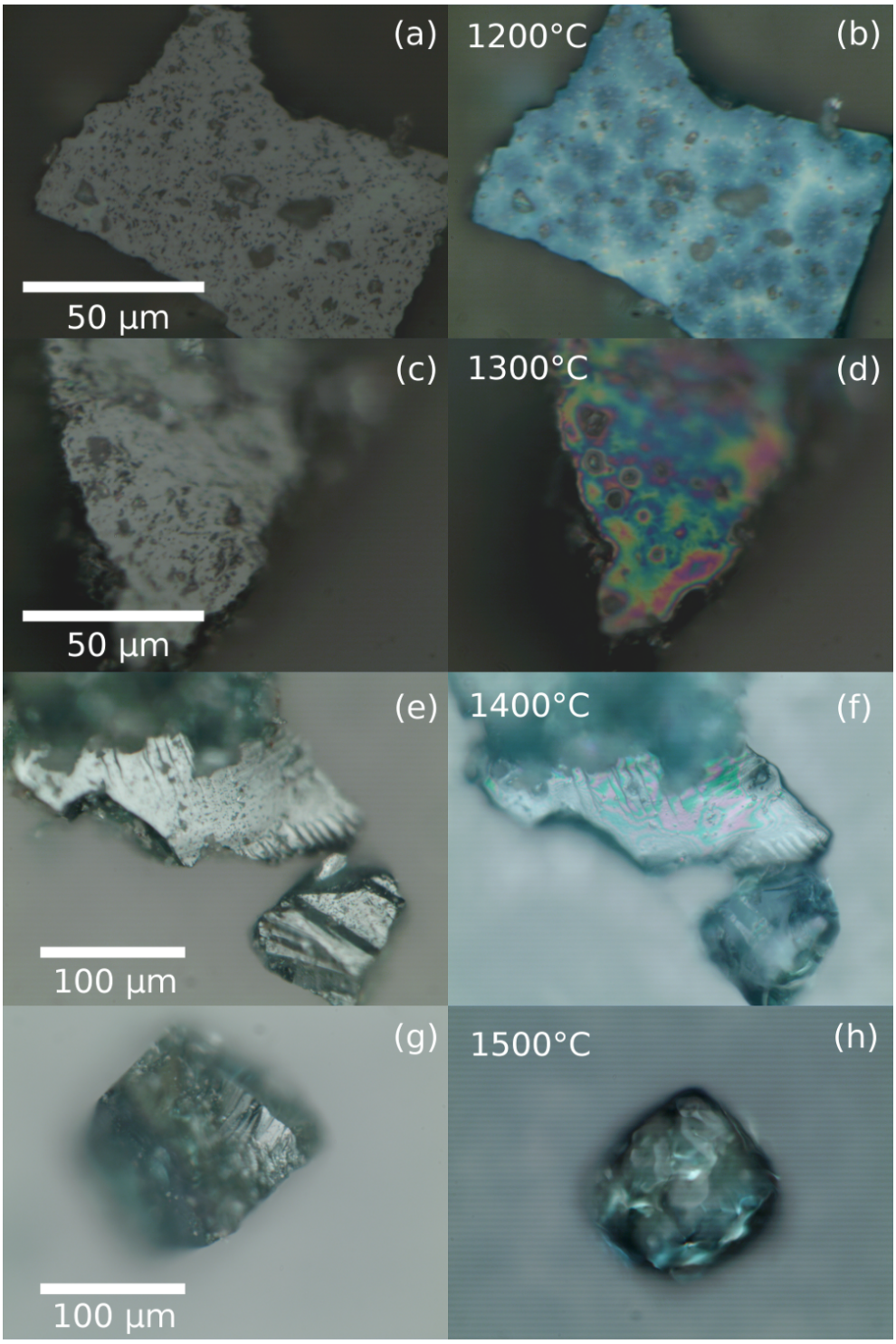

Figure 8. Overview of the results of oxidizing 4H SiC powder at four separate temperatures in an argon-water vapor mix for 2 h. Images on the left show the particles before oxidation and the images on the right show particles after oxidation. Note that the lower two pairs of images have been taken at lower magnification than that of the top two pairs. The same particle is pictured in the before and after pictures for the top three pairs, but the particles shown from the 1500 °C oxidation run have not been confirmed to be the same.

[11] Houlton, J., Chen, M., Brubaker, M., Bertness, K., and Rogers, C., "Axisymmetric scalable magneto-gravitational trap for diamagnetic particle levitation," *Rev. of Sci. Instrum.* **89**(12), 125107 (2018).
[12] La Porta, A. and Wang, M. D., "Optical torque wrench: angular trapping, rotation, and torque detection of quartz microparticles," *Phys. Rev. Lett.* **92**(19), 190801 (2004).
[13] Arita, Y., Mazilu, M., and Dholakia, K., "Laser-induced rotation and cooling of a trapped microgyroscope in vacuum," *Nature Commun.* **4**, 2374 (2013).
[14] Monteiro, F., Ghosh, S., van Assendelft, E. C., and Moore, D. C., "Optical rotation of levitated spheres in high vacuum," *Phys. Rev. A* **97**(5), 051802 (2018).
[15] Delord, T., Nicolas, L., Schwab, L., and Hétet, G., "Electron spin resonance from NV centers in diamonds levitating in an ion trap," *New. J. Phys.* **19**(3), 033031 (2017).
[16] Yin, Z.-q., Li, T., Zhang, X., and Duan, L., "Large quantum superpositions of a levitated nanodiamond through spin-optomechanical coupling," *Phys. Rev. A* **88**(3), 033614 (2013).
[17] Milatz, J., Van Zolingen, J., and Van Iperen, B., "The reduction in the brownian motion of electrometers," *Physica* **19**(1-12), 195–202 (1953).
[18] Courty, J.-M., Heidmann, A., and Pinard, M., "Quantum limits of cold damping with optomechanical coupling," *Eur. Phys. J. D* **17**(3), 399–408 (2001).
[19] Li, T., "Millikelvin cooling of an optically trapped microsphere in vacuum," in [*Fundamental Tests of Physics with Optically Trapped Microspheres*], 81–110, Springer (2013).
[20] Jain, V., Gieseler, J., Moritz, C., Dellago, C., Quidant, R., and Novotny, L., "Direct measurement of photon recoil from a levitated nanoparticle," *Phys. Rev. Lett.* **116**(24), 243601 (2016).
[21] Tebbenjohanns, F., Frimmer, M., Militaru, A., Jain, V., and Novotny, L., "Cold damping of an optically levitated nanoparticle to micro-Kelvin temperatures," *arXiv:1812.09875* (2018).
[22] Cavendish, H., "Experiments to determine the density of the earth," *Phil. Trans.* **88**, 469 (1798).
[23] Gillies, G. T., "The Newtonian gravitational constant: An index of measurements," *Metrologia* **24**, 1 (1987).
[24] Horstman, K. and Trimble, V., "A citation history of measurements of Newton's constant of gravity," *arXiv:1811.10556* (2018).
[25] Quinn, T., "Fundamental constants: Measuring big G," *Nature* **408**, 919 (2000).
[26] Holzschuh, E., Kündig, W., Nolting, F., Pixley, R., Schurr, J., Straumann, U., et al., "Measurement of newtons gravitational constant," *Phys. Rev. D* **74**(8), 082001 (2006).
[27] Parks, H. V. and Faller, J. E., "Simple pendulum determination of the gravitational constant," *Phys. Rev. Lett.* **105**(11), 110801 (2010).
[28] Fixler, J. B., Foster, G., McGuirk, J., and Kasevich, M., "Atom interferometer measurement of the newtonian constant of gravity," *Science* **315**(5808), 74–77 (2007).
[29] Gundlach, J. H. and Merkowitz, S. M., "Measurement of newton's constant using a torsion balance with angular acceleration feedback," *Phys. Rev. Lett.* **85**, 2869–2872 (Oct 2000).
[30] Luo, J., Liu, Q., Tu, L.-C., Shao, C.-G., Liu, L.-X., Yang, S.-Q., Li, Q., and Zhang, Y.-T., "Determination of the Newtonian gravitational constant G with time-of-swing method," *Phys. Rev. Lett.* **102**, 240801 (Jun 2009).
[31] DeSalvo, R., "Unaccounted source of systematic errors in measurements of the Newtonian gravitational constant G," *Phys. Lett. A* **379**, 1202 (2015).
[32] Paul, W., "Electromagnetic traps for charged and neutral particles," *Rev. of Mod. Phys.* **62**(3), 531 (1990).
[33] Jiang, L., Whitten, W. B., and Pau, S., "A planar ion trapping microdevice with integrated waveguides for optical detection," *Opt. Express* **19**(4), 3037–3043 (2011).
[34] Jennings, V. J., "The etching of silicon carbide," *Mater. Res. Bull.* **4**, S199 (1969).
[35] Chu, T. L. and Campbell, R. B., "Chemical etching of silicon carbide with hydrogen," *J. Electrochem. Soc.* **112**, 955 (1965).
[36] Harris, J. M., Gatos, H. C., and Witt, A. F., "Etching characteristics of silicon carbide in hydrogen," *J. Electrochem. Soc.* **116**, 380 (1969).
[37] Kumagawa, M. and Kuwabara, H., "Hydrogen etching of silicon carbide," *Jpn. J. Appl. Phys.* **8**, 421 (1969).
[38] Owman, F., Hallin, C., Martensson, P., and Janzén, E., "Removal of polishing-induced damage from 6H-SiC (0001) substrates by hydrogen etching," *J. Cryst. Growth* **167**, 391 (1996).

[39] Ramachandran, V., Brady, M. F., Smith, A. R., Feenstra, R. M., and Greve, D. W., "Preparation of atomically flat surfaces on silicon carbide using hydrogen etching," *J. Electron. Mater.* **27**, 308 (1998).

[40] Soubatch, S., Saddow, S. E., Rao, S. P., Lee, W. Y., Konuma, M., and Starke, U., "Structure and morphology of 4H-SiC wafer surfaces after H_2-etching," *Mater. Sci. Forum* **483–485**, 761 (2005).

[41] Frewin, C. L., Coletti, C., Riedl, C., Starke, U., and Saddow, S. E., "A comprehensive study of hydrogen etching on the major SiC polytypes and crystal orientations," *Mater. Sci. Forum* **615–617**, 589 (2009).

[42] Ishida, Y. and Yoshida, S., "Investigation of the giant step bunching induced by the etching of 4H-SiC in Ar-H_2 mix gases," *Jpn. J. Appl. Phys.* **55**, 095501 (2016).

[43] Ishida, Y. and Yoshida, S., "Proposal of quasi thermal equilibrium model for etching phenomenon by gases: Example of the etching of 4H-SiC by H_2," *Jpn. J. Appl. Phys.* **53**, 046501 (2014).

[44] Brady, E. L., "Chemical nature of silica carried by steam," *J. Phys. Chem.* **57**, 706 (1957).

[45] Opila, E. J. and Hann, R. H., "Paralinear oxidation of CVD SiC in water vapor," *J. Am. Ceram. Soc.* **80**, 197 (1997).

[46] Opila, E. J., "Oxidation and volatilization of silica formers in water vapor," *J. Am. Ceram. Soc.* **86**, 1238 (2003).

[47] Wagner, C., "Beitrag zur theorie des anlaufvorgangs," *Z. Phys. Chem.* **21B**, 25 (1955).

[48] Mott, N. F., "The theory of the formation of protective oxide films on metals–III," *Trans. Faraday Soc.* **43**, 429 (1947).

[49] Lide, D. R., ed., [*CRC Handbook of Chemistry and Physics*], CRC Press, 85 ed. (2004).